

---

# MACL: MULTI-LABEL ADAPTIVE CONTRASTIVE LEARNING LOSS FOR REMOTE SENSING IMAGE RETRIEVAL

---

**Amna Amir**

Faculty of Engineering and Natural Sciences  
VPA Lab  
Sabanci University  
Istanbul, Türkiye  
amna.butt@sabanciuniv.edu

**Erchan Aptoula**

Faculty of Engineering and Natural Sciences  
VPA Lab  
Sabanci University  
Istanbul, Türkiye  
erchan.aptoula@sabanciuniv.edu

## ABSTRACT

Semantic overlap among land-cover categories, highly imbalanced label distributions, and complex inter-class co-occurrence patterns constitute significant challenges for multi-label remote-sensing image retrieval. In this article, Multi-Label Adaptive Contrastive Learning (MACL) is introduced as an extension of contrastive learning to address them. It integrates label-aware sampling, frequency-sensitive weighting, and dynamic-temperature scaling to achieve balanced representation learning across both common and rare categories. Extensive experiments on three benchmark datasets (DLRSD, ML-AID, and WHDL), show that MACL consistently outperforms contrastive-loss based baselines, effectively mitigating semantic imbalance and delivering more reliable retrieval performance in large-scale remote-sensing archives. Code, pretrained models, and evaluation scripts will be released at <https://github.com/amna/MACL> upon acceptance.

**Keywords** Multi-label · contrastive learning · remote sensing · content-based image retrieval.

## 1 Introduction

The evolution of remote sensing technologies has significantly increased the daily volume of satellite imagery acquisition, resulting in vast archives that require efficient data management solutions[1]. Content-based image retrieval (CBIR) addresses this challenge by retrieving images from large databases based on their visual content rather than on textual or metadata descriptions[2]. In this process, discriminative features are extracted from both the query images and the images stored in the database, after which similarity measures are computed to retrieve the most relevant results.

However, the application of CBIR to remote sensing imagery is particularly challenging [3], since remote sensing scenes are characterized by intricate spatial structures, highly variable object scales, and diverse spectral characteristics, where each image is often composed of multiple land-cover types or semantic classes that are spatially co-occurring and overlapping. Consequently, *multi-label* CBIR, where each sample is associated with an arbitrary number of labels, is considered a more realistic paradigm [4, 5, 6].

Notable approaches in this regard include fully convolutional networks extracting pixel-level features [7], deep hashing methods compressing high-dimensional features into compact binary codes for efficient retrieval [8, 9] and graph-based strategies capturing inter-class relationships [10]. Nevertheless, all aforementioned methods were limited by predefined similarity measures and the static nature of graph structures. Which is why, *contrastive learning* (CL) [11], as a data-driven representation learning paradigm has become immensely a popular for retrieval purposes [12]. Within CL, feature embeddings are learned by maximizing the agreement between semantically similar samples while minimizing similarity between dissimilar ones, leading to compact intra-class and well-separated inter-class representations.

There are various reported cases of CL based CBIR solutions for remote sensing [13], showing its ability to capture semantic similarity relations. However, most existing approaches have been developed under single-label assumptions, where each image is assumed to represent a single concept [14]. Attempts to extend CL to multi-label settings have been made [15, 16, 17], where the main challenge arises from the ambiguities in defining positive and negative pairs

given the multitude of labels per sample. Still, they ignore category co-occurrence frequencies and class balances, thus limiting their potential.

In this article, a multi-label extension to supervised CL is proposed, named *Multi-Label Adaptive Contrastive Learning* (MACL), aiming for balanced and relationship-aware representation learning. It incorporates adaptive mechanisms to adjust the learning process according to label relationships and category frequency. MACL supports label-aware sampling for balanced pair formation, frequency-sensitive weighting to highlight rare categories, and dynamic-temperature scaling to adjust similarity sensitivity based on semantic overlap. Extensive experiments on three benchmark datasets (DLRSD, ML-AID, and WHDL), show that MACL consistently outperforms CL based baselines, effectively mitigating semantic imbalance and delivering more reliable retrieval performance in large-scale remote-sensing archives.

## 2 Related Work

### 2.1 Single-Label Remote Sensing Image Retrieval (SLRSIR)

SLRSIR has been developed to retrieve remote sensing scenes assumed to represent a single semantic concept. Among the large volume of existing methods in this regard, the most notable include deep metric and triplet-based learning networks, that have been used to optimize intra-class compactness and inter-class separability [18, 19, 20]. In particular, dual-anchor triplet loss and global-aware ranking strategies have been reported to strengthen the discriminative capability of learned embeddings [21]. A learnable joint spatial-spectral transformation has also been proposed to enhance image representation [22].

Moreover, attention and graph-based frameworks have also been studied intensively. Specifically,

multi-attention fusion networks with dilated convolution and label smoothing have been developed to capture multi-scale contextual cues while suppressing redundant information [23]. In addition, attention-driven graph convolutional networks have been proposed to model spatial dependencies among image patches, leading to context-aware representations that significantly improve retrieval robustness [24]. A self-attention feature metric learning framework has also been introduced to jointly leverage attention mechanisms and metric learning, effectively enhancing the discriminative power of learned features and semantic alignment [25].

As far as efficiency is concerned, large-scale retrieval systems have often adopted hashing and meta-learning paradigms. In detail, asymmetric hash code learning frameworks have been employed to generate discriminative binary codes without compromising accuracy [26]. Meta hashing strategies have also been developed to adapt hash functions dynamically to new data distributions [27]. Adaptive hash-code balancing frameworks have addressed in particular the imbalance and difficulty spectrum among image pairs in SLRSIR, resulting in more robust retrieval over varied categories [28]. These developments have provided a balance between retrieval speed and semantic precision, making them suitable for real-world SLRSIR systems.

Furthermore, plasticity-stability preserving multi-task frameworks have been proposed to retain previously acquired representations while adapting to new data [29]. Besides, centripetal-intensive deep hashing [30] and deep attention hashing with distance-adaptive ranking have advanced hybrid learning between metric and hashing paradigms, improving semantic compactness and retrieval precision [31]. However, despite the strong progress of SLRSIR, their assumption of one dominant category per image has restricted their applicability to complex remote sensing scenes that typically contain multiple semantic concepts.

### 2.2 Multi-Label Remote Sensing Image Retrieval (MLRSIR)

MLRSIR addresses the content-based retrieval of satellite scenes with multiple co-occurring semantic elements [6]. Each image typically contains several land cover categories such as residential areas, roads, vegetation, or water, which have appeared at different spatial scales and formed highly heterogeneous scene compositions [32], that complicate learning accurate representations reflecting image similarity [5]. Furthermore, the distribution of land cover classes is often imbalanced, thus hindering the learning of balanced retrieval embeddings [33].

Notable approaches to MLRSIR include graph based frameworks that have been proposed to model label dependencies and spatial relationships [34, 35, 10], while reconstruction and segmentation driven pipelines have performed retrieval using region or pixel level masks [36]. Region convolutional and fully convolutional feature extraction schemes have also been developed to enhance spatially localized retrieval performance [7]. Moreover, attention based and transformer based architectures have also been investigated to capture contextual information and long range dependencies among labels [37].

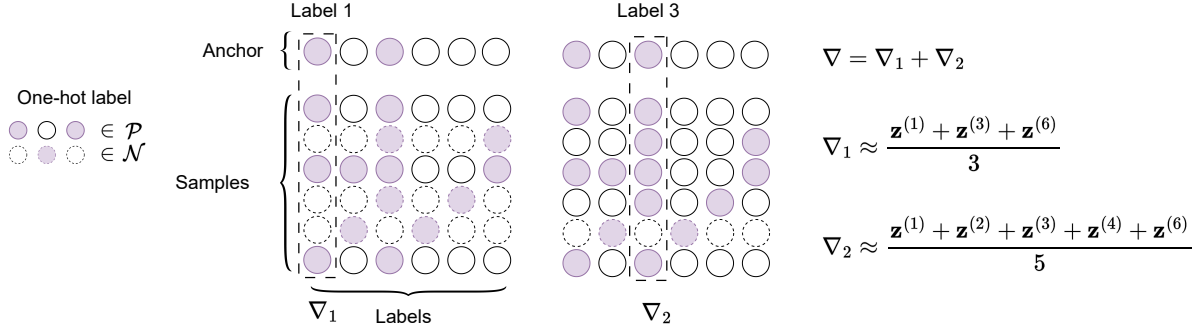


Figure 1: Illustration of the MulSupCon method. Each row represents a sample’s one-hot label vector, with the first row being the anchor sample (top row) and the remaining rows corresponding to other samples in the batch. Filled circles indicate active label dimensions. Samples enclosed with dotted outlines belong to the negative set  $\mathcal{N}$ , while the remaining samples form the positive set  $\mathcal{P}$ . For an anchor with labels  $\{1, 3\}$ , the corresponding positive sets are  $P_1 = \{1, 3, 6\}$  and  $P_3 = \{1, 2, 3, 4, 6\}$ , which form the basis for label-wise contrastive learning in MulSupCon.

Despite the progress achieved by these architectural approaches, their performance remains constrained by the quality of the underlying feature space. As a result, increased attention has been directed toward multi-label contrastive learning, which offers a principled mechanism for representing semantic overlap and inter-label relationships more effectively.

### 2.3 Multi-label contrastive learning

Multi-label contrastive learning was initially developed within computer vision, and its principles have been considered applicable to MLRSIR, where images are characterized by multiple co-occurring categories, imbalanced label distributions, and complex label relationships. Earlier MLRSIR research has been primarily directed toward architectural designs, while contrastive and metric-learning formulations have been recognized as a strong alternative for improving multi-label feature representations. Their general and flexible objectives, originally developed for multi-label image understanding, have been adapted to remote sensing image retrieval, particularly in scenarios defined by diverse label co-occurrence patterns and long-tailed distributions.

A large portion of existing approaches are based on the foundational Supervised Contrastive Learning (SupCon) objective [14], which encourages semantically similar samples to be grouped in embedding space. Because SupCon was designed for single-label supervision, multi-label variants have mainly differed in the definition of positive samples and in the weighting of label relationships. Early extensions follow two simple strategies: SupCon-ALL, which treats samples as positives only when their complete label sets match, and SupCon-ANY, which treats samples as positives when they share at least one label. These strategies represent strict and inclusive supervision, but they do not reflect differences in the strength of partial semantic overlap. More refined approaches have therefore been developed. Soft-weighting schemes such as LBase [38] use Jaccard similarity to assign continuous weights according to label-set overlap. Prototype-based methods such as LProto [39] shift learning toward instance-prototype alignment, producing more stable class-level representations. Label-wise strategies such as MulSupCon [15] and its weighted variant treat each label of a sample as a separate anchor, providing finer supervision and more balanced gradients for samples with many labels. Beyond simple overlap metrics, some formulations incorporate structural or distributional properties of label space. LMSC [38] uses prototypes, memory queues, and frequency-aware reweighting to address long-tailed label distributions. LReg [17] introduces gradient regularization to reduce conflicts among correlated labels, while SimDis [16] models both similarity and dissimilarity through label intersections and complements to provide finer semantic control.

Despite their differences, these methods rely on two central design choices: how positive samples are defined and how label-dependent weighting influences attraction and repulsion during contrastive learning. However, most existing methods still depend on static assumptions regarding label relations, typically expressed through overlap counts, binary relevance matrices, or predefined graphs. This static treatment limits the ability of these models to handle label imbalance, semantic variability, and uneven co-occurrence frequencies, all of which are pronounced in remote sensing imagery.

These observations have motivated the development of a more adaptive contrastive formulation that can adjust similarity forces according to label rarity, semantic consistency, and sample complexity. In response, the Multi-Label Adaptive

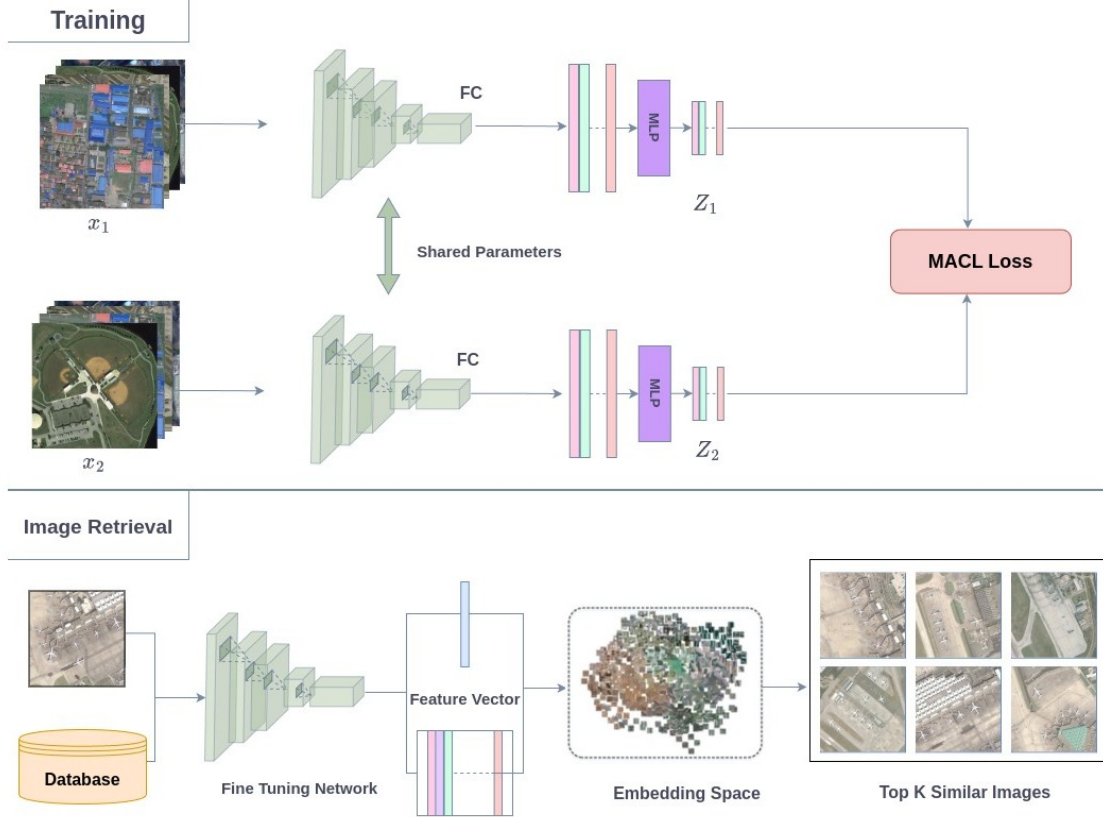


Figure 2: Training and retrieval pipeline employing the proposed MACL loss. During training, images are encoded by a shared backbone and projection head to produce embeddings optimized using the MACL loss. During retrieval, query and database images are embedded into a common feature space and ranked based on similarity.

Contrastive Learning (MACL) framework is introduced, in which adaptive weighting and dynamic temperature scaling are used to better align multi-label relationships and improve retrieval performance in remote sensing scenarios.

### 3 MACL

The MACL framework is designed to overcome the limitations of existing multi-label contrastive methods which rely on uniform pair weighting and fixed temperature scaling. MACL introduces two adaptive mechanisms, Pairwise Label Reweighting (PLR) and Dynamic Temperature Scaling (DTS), allowing the loss to incorporate semantic imbalance, label co-occurrence, and inter-class relationship awareness within contrastive learning.

**Motivation:** MLRSIR presents unique challenges: labels are overlapping, imbalanced, and strongly correlated. Standard SupCon is inherently limited to single-label settings. MulSupCon extends SupCon to multi-label data by decomposing each anchor into multiple label-specific anchors and treating samples sharing that label as positives, but it still relies on simplifying assumptions. To visually demonstrate how MulSupCon constructs label-wise positive sets and applies uniform contributions, Fig. 1 is presented as a schematic illustration, which also facilitates a smoother transition into the limitations discussed next.

These assumptions are problematic in remote sensing because frequent classes (e.g., *building*, *road*) dominate gradients, rare but informative classes (e.g., *airplane*, *harbor*) are underrepresented, and semantic proximity varies widely (e.g., *residential*  $\leftrightarrow$  *road* vs. *harbor*  $\leftrightarrow$  *stadium*).

Case 1 (Unequal semantic overlap): An anchor labeled  $\{building, road, tree\}$  compared with a sample labeled  $\{building\}$  should be considered less similar to it than when compared with a sample labeled  $\{building, road, tree\}$ , yet conventional losses treat both pairs equally.

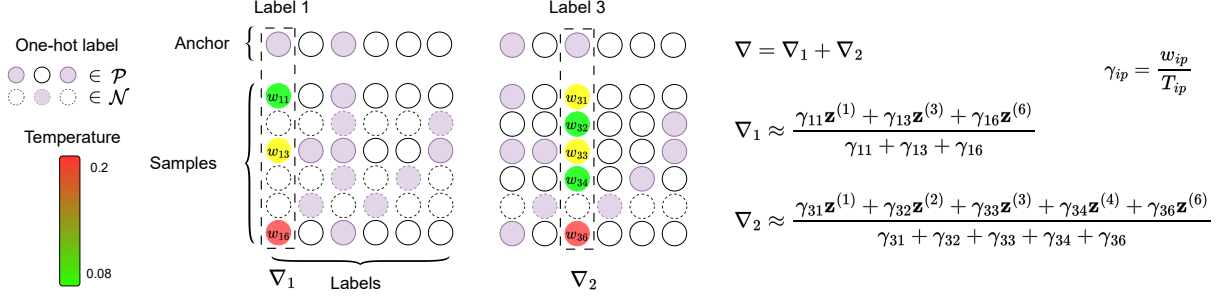


Figure 3: Visualization of the MACL mechanism. For each anchor label, MACL computes a label-specific gradient component using pairwise weights (green/yellow/red nodes) and adaptive temperatures (color bar). The effective influence of each positive is determined by  $\gamma_{ip} = w_{ip}/T_{ip}$ , and the final gradient is obtained by combining the label-specific components.

Case 2 (Rare vs. frequent classes): Pairs involving common labels (e.g., *pavement*) dominate training, while rare but critical labels (e.g., *airplane*) contribute little, biasing embeddings in favor of frequent classes.

The introduction of MACL is motivated by the fact that uniform pair treatment fails to capture semantic imbalance, rarity, and heterogeneous label interactions. MACL is formulated as a generalization that replaces uniform pair treatment with adaptive, relationship-aware optimization. Positive pairs within each label-specific set vary in importance and semantic strength, and their contributions are determined by label rarity, semantic overlap, and co-occurrence patterns, thereby aligning optimization with the intrinsic structure of multi-label data.

**MACL Architecture and Workflow.** As illustrated in Fig. 2, MACL follows an embedding-based contrastive learning paradigm. During training, images within a mini-batch are processed by a shared backbone encoder followed by a projection head, producing normalized feature embeddings in a shared representation space. For each anchor image, all remaining samples in the batch act as comparisons, forming label-dependent positive and negative sets according to their multi-label annotations. The proposed MACL loss is then applied to these embeddings, adaptively modulating pairwise interactions through PLR and DTS.

At inference time, the trained encoder is used to embed both query and database images into the same feature space. Image retrieval is performed by ranking database embeddings based on similarity to the query embedding, without requiring label information. This unified architecture ensures that the adaptive contrastive optimization learned during training directly translates to improved retrieval performance under multi-label supervision.

In contrast to traditional contrastive methods, which treat all positive pairs uniformly, MACL treats each pair as a unique learning relationship with distinct importance and difficulty. This is accomplished through two synergistic mechanisms: PLR and DTS.

Before the mechanisms are introduced, the notation used throughout the formulation is summarized for clarity.

**Notation:** The embedding of the anchor sample is written as  $\mathbf{z}_q^{(i)}$ , and the embedding of any comparison is  $\mathbf{z}_k^{(a)}$ . The pairwise similarity is expressed as  $s_{ia} = \mathbf{z}_q^{(i)} \cdot \mathbf{z}_k^{(a)}$ , and the set of samples compared with anchor  $i$  is represented by  $A(i)$ . The label set associated with sample  $i$  is denoted by  $y^{(i)}$ , and the number of labels assigned to that sample is written as  $|y^{(i)}|$ . A specific label within this set is referred to as  $y_j^{(i)}$ , indicating the  $j$ th label of sample  $i$ .

**PLR:** It establishes a *rarity-aware importance hierarchy* by assigning each anchor–positive pair  $(i, p)$  a weight  $w_{ip}$  that reflects the informativeness of their shared labels. The pairwise weight  $w_{ip}$  quantifies how rare the shared labels are between anchor  $i$  and positive sample  $p$  and is computed using the label-intersection frequency function  $f(y^{(i)}, y^{(p)})$ , which measures how often the two label sets co-occur in the dataset. Rare co-occurrences lead to larger weights:

$$w_{ip} = \frac{1}{\log(1 + f(y^{(i)}, y^{(p)})) + \epsilon} \quad (1)$$

This weighting ensures that informative, low-frequency relationships exert stronger influence than common label pairs.

**DTS:** It introduces *semantic-aware similarity calibration* by recognizing that different label combinations require different similarity thresholds. The pairwise temperature  $T_{ip}$  adapts the similarity calibration based on two components: the semantic-overlap measure  $J(y^{(i)}, y^{(p)})$ , which quantifies how similar the two label sets are, and the marginal frequency  $h(y^{(i)})$ , which represents how rare anchor  $i$ 's labels are in the dataset. This relationship is formally defined as:

$$T_{ip} = \underbrace{\exp(-\alpha J(y^{(i)}, y^{(p)}))}_{\text{Term 1: Pair Overlap}} + \beta \underbrace{\left( \frac{1}{\log(1 + h(y^{(i)}))} \right)}_{\text{Term 2: Anchor Rarity}} \quad (2)$$

High semantic overlap results in lower temperatures, while rare anchors receive additional temperature increases to stabilize optimization. This adaptive temperature encourages sharper boundaries for semantically close pairs and smoother ones for weakly related pairs.

Here,  $J(\cdot)$  denotes the semantic-overlap measure,  $h(\cdot)$  denotes the marginal label frequency, and  $\alpha$  and  $\beta$  control semantic emphasis and rarity weighting, respectively. Together, PLR and DTS establish a heterogeneous similarity landscape in which each anchor–positive pair contributes according to its semantic strength, rarity, and contextual informativeness.

As shown in Fig. 3, MACL assigns each positive a weighted and temperature-scaled contribution, determining how strongly that sample influences the anchor. This produces heterogeneous, label-aware gradients that reflect semantic overlap, rarity, and pairwise informativeness.

The family of supervised contrastive learning methods is generalized by MACL. Classical methods such as SupCon, MulSupCon, and LBase appear as special cases when PLR weights are set to  $w_{ip} = 1$  and DTS temperatures are fixed to a constant  $\tau$ . Through adaptive weighting and temperature scaling, MACL expands the contrastive optimization space beyond uniform objectives.

This expanded flexibility is reflected in several ways:

- Each pair's contribution is determined by semantic relatedness and label rarity, producing a gradient field aligned with multi-label structure.
- Gradient flow varies across the embedding space based on pair difficulty instead of uniformly across all positives.
- Convergence is shaped jointly by global label statistics and local semantic interactions.

**MACL loss Formulation:** MACL extends MulSupCon by incorporating its two adaptive mechanisms (PLR and DTS) into each label-wise contrastive component. For each  $y_j^{(i)} \in \mathbf{y}^{(i)}$ , a separate positive set has been constructed:

$$P_j^{(i)} = \{ m \mid \forall m, y_j^{(i)} \in y^{(m)} \} \quad (3)$$

For anchor  $i$  with label set  $\mathbf{y}^{(i)}$ , MACL loss is defined as:

$$\mathcal{L}_{\text{MACL}} = \sum_{y_j^{(i)} \in \mathbf{y}^{(i)}} \frac{-1}{|P_j^{(i)}|} \sum_{p \in P_j^{(i)}} w_{ip} \log \frac{\exp(s_p^{(i)}/T_{i,p})}{\sum_{a \in A^{(i)}} \exp(s_a^{(i)}/T_{i,a})} \quad (4)$$

Here,  $w_{ip}$  and  $T_{ip}$  are the PLR and DTS terms, respectively, determining the adaptive strength and weighting of each positive relationship. Fig. 3 visualizes how these pair-specific terms produce non-uniform contributions across label-dependent positive sets.

MACL discovers and exploits the inherent heterogeneity of multi-label relationships. Contrastive learning from a rigid, uniform process into a flexible, adaptive optimization that respects the complexity of real-world multi-label data. From a geometric perspective MACL creates a dynamic embedding space where the interaction structure of attraction and repulsion is continuously modulated based on relationship properties. The embedding space exhibits adaptive spatial structure where important relationships create stronger gradients and semantically rich pairs form tighter clusters.

**Gradient Analysis of MACL:** The behavior of MACL in the embedding space can be examined by analyzing the gradient of the loss with respect to the anchor embedding  $\mathbf{z}_q^{(i)}$ . The MACL objective is given by

$$\mathcal{L}_{\text{MACL}}^{(i)} = \sum_{y_j^{(i)} \in y^{(i)}} \frac{-1}{|P_j^{(i)}|} \sum_{p \in P_j^{(i)}} w_{ip} \log \frac{\exp(s_{ip}/T_{ip})}{\sum_{a \in A(i)} \exp(s_{ia}/T_{ia})} \quad (5)$$

where

$$s_{ia} = \mathbf{z}_q^{(i)} \cdot \mathbf{z}_k^{(a)} \quad (6)$$

Substituting this relation yields the gradient expression:

$$\begin{aligned} \nabla_{\mathbf{z}_q^{(i)}} \mathcal{L}_{\text{MACL}}^{(i)} &= \sum_{y_j^{(i)} \in y^{(i)}} \left[ -\frac{1}{|P_j^{(i)}|} \sum_{p \in P_j^{(i)}} \frac{w_{ip}}{T_{ip}} \mathbf{z}_k^{(p)} \right] \\ &+ |y^{(i)}| \left[ \sum_{a \in A(i)} \frac{1}{T_{ia}} \frac{\exp(s_{ia}/T_{ia})}{C} \mathbf{z}_k^{(a)} \right] \end{aligned} \quad (7)$$

The adaptive attraction term for label  $y_j^{(i)}$  is defined as:

$$\bar{\mathbf{z}}_j^{\text{MACL}} = -\frac{1}{|P_j^{(i)}|} \sum_{p \in P_j^{(i)}} \frac{w_{ip}}{T_{ip}} \mathbf{z}_k^{(p)} \quad (8)$$

while the adaptive repulsion term is expressed as:

$$\hat{\mathbf{z}}^{\text{MACL}} = \sum_{a \in A(i)} \frac{1}{T_{ia}} \frac{\exp(s_{ia}/T_{ia})}{C} \mathbf{z}_k^{(a)} \quad (9)$$

Combining these components yields the compact gradient form

$$\nabla_{\mathbf{z}_q^{(i)}} \mathcal{L}_{\text{MACL}}^{(i)} = \sum_{y_j^{(i)} \in y^{(i)}} \bar{\mathbf{z}}_j^{\text{MACL}} + |y^{(i)}| \cdot \hat{\mathbf{z}}^{\text{MACL}} \quad (10)$$

The vector  $\bar{\mathbf{z}}_j^{\text{MACL}}$  acts as a label-specific adaptive representation, aggregating positive samples in proportion to their rarity and semantic closeness. The repulsion vector  $\hat{\mathbf{z}}^{\text{MACL}}$  prevents collapse by distributing temperature-scaled force across all comparisons.

For any sample  $t$  sharing the label intersection  $y = y^{(i)} \cap y^{(t)}$ , the total attraction is:

$$-\sum_{y_j \in y} \frac{w_{it}}{T_{it}} \frac{1}{|P_j^{(i)}|}$$

This shows that samples with greater semantic strength exert stronger pull, while common or weakly related samples contribute less influence.

**Complexity:** MACL introduces pair-specific weights and temperatures, resulting in  $\mathcal{O}(B^2)$  computational complexity for batch size  $B$ . Label co-occurrence statistics and overlap computations are precomputed and cached, ensuring minimal runtime overhead. In practice, the added computations are lightweight and do not significantly impact runtime.

Overall, MACL transforms multi-label contrastive learning from a uniform interaction model into a fully adaptive, relationship-aware framework. By tailoring gradients to semantic relevance, rarity, and label overlap, MACL produces a structured embedding space that aligns with the heterogeneous nature of real-world multi-label data.

Table 1: Summary of selected MLRSIR datasets.

Dataset	No. of Labels	No. of Images	Image Size	Resolution (m)	Image Source	Year
DLRSD[40]	17	2,100	256×256	0.3	DLRSD	2018
ML-AID[41]	17	3,000	600×600	8–0.5	AID	2020
WHDL D[7]	6	4,940	256×256	2	Gaofen-1 and Ziyuan-3	2020

## 4 Experiments

The experiments have been conducted with the goal of evaluating MACL against existing supervised contrastive losses on standard ML-RSIR benchmarks (Tables 1).

### 4.1 Datasets and splitting

**DLRSD** [40]: provides aerial images annotated with binary multi-hot vectors across 21 land-use categories. It is widely used in multi-label remote sensing because it captures diverse urban and natural scenes at high spatial resolution.

**ML-AID** [41]: extends the AID dataset with multi-label annotations, enabling evaluation of both classification and retrieval tasks. Each image is annotated with multiple land-cover classes, and labels are provided in CSV format.

**WHDL D** [7]: is a dense pixel-level labeling dataset derived from Gaofen-1 and Ziyuan-3 imagery. Unlike DLRSD and ML-AID, it provides annotations for six primitive land-cover categories, making it suitable for both image-level and pixel-level analysis.

Table 2: Overview of dataset train/val/test splits.

Dataset	#Images	#Labels	Train	Validation	Test
DLRSD	2,100	17	1,475	214	411
ML-AID	3,000	17	2,100	300	600
WHDL D	4,940	6	3,444	518	978

Following the approach in [6], all datasets are partitioned using a fixed 70/10/20 ratio for training, validation, and testing, respectively. The splits are generated randomly for each dataset (Table 2). In the retrieval stage, each test image is used once as a query, and the remaining test images form the gallery. This setup ensures consistent and fair evaluation across datasets with different sizes, label distributions, and spatial resolutions.

### 4.2 Implementation Details

The framework was developed using ResNet-18 as the backbone and a two-layer projection head. To enhance the diversity of training data and improve model robustness, several augmentations were applied, including random resized cropping, horizontal and vertical flipping, small-angle rotations, and color jittering. Examples of augmented samples for each dataset are shown in Figs. 4, 5, and 6. In practice, MACL has training and inference costs comparable to MulSupCon, since PLR and DTS only introduce lightweight pairwise computations without altering backbone architecture or feature dimensionality.

Model training was conducted on an NVIDIA GeForce GTX 1660 Ti GPU with 6 GB of memory. Each model underwent 100 epochs of training. The process used the Adam optimizer (learning rate of 0.001, temperature of 0.3, weight decay of 0.0005) with a batch size of 128. Additionally, a CosineAnnealingLR scheduler lowered the learning rate by 20% every 15 epochs, and gradient clipping (with a maximum norm of 1.0) was applied to prevent exploding gradients. For numerical stability, The value  $\epsilon = 10^{-8}$  was set in PLR to avoid division by zero. In DTS,  $\alpha = 1.5$  was set to control the influence of semantic similarity, and  $\beta = 0.1$  was set to amplify the effect of rare labels. All hyperparameters were selected empirically based on validation performance and stability considerations.

### 4.3 Evaluation Metrics

Retrieval performance is evaluated using two categories of metrics: cosine-similarity-based metrics for ranking quality in the learned embedding space, and Jaccard-similarity-based metrics for multi-label relevance assessment.

Table 3: Overview of the DLRSD, ML-AID, and WHDL D datasets, including class names and the no. of images per label.

Label	DLRSD Class	No. of Images	ML-AID Class	No. of Images	WHDL D Class	No. of Images
1	airplane	100	bare soil	1475	building	3722
2	bare soil	754	airplane	99	road	3162
3	building	713	building	2161	pavement	3881
4	car	897	car	2026	vegetation	4631
5	chaparral	116	chaparral	112	bare soil	3539
6	court	105	court	344	water	3886
7	dock	100	dock	271	–	–
8	field	103	field	214	–	–
9	grass	977	grass	2295	–	–
10	mobile home	102	mobile home	2	–	–
11	pavement	1331	pavement	2328	–	–
12	sand	291	sand	259	–	–
13	sea	101	sea	221	–	–
14	ship	103	ship	284	–	–
15	tank	100	tank	108	–	–
16	tree	1021	tree	2406	–	–
17	water	208	water	852	–	–

#### 4.3.1 Cosine-Similarity Based Metrics

Cosine-similarity-based metrics evaluate ranking quality in the learned embedding space by comparing feature vectors of query and database images. Two points are considered similar if they belong to the same category or share at least one tag. Following [42],  $mAP@5000$  computes the mean average precision over the top-5000 retrieved results. The  $nDCG@100$  assesses the top-100 ranking using graded relevance, with  $IDCG@K$  denoting the ideal ordering for  $k = 100$ .

$$\begin{aligned}
 P@n &= \frac{\#\{\text{relevant images in top } N \text{ results}\}}{N} \\
 AP &= \frac{\sum_n P@n \times I\{\text{image } n \text{ is relevant}\}}{\#\{\text{retrieved relevant images}\}} \\
 mAP &= \frac{1}{Q} \sum_i AP_i
 \end{aligned} \tag{11}$$

where  $\#$  indicates a count function,  $I$  denotes an indicator function, and  $Q$  is the total number of queries. The  $mAP$  is computed from the retrieval list over the entire database, whereas  $mAP@n$  is calculated from only the top- $n$  retrieved results.

$$nDCG@p = \frac{1}{Z} \sum_{i=1}^p \frac{2^{r_i} - 1}{\log(1 + i)} \tag{12}$$

where  $Z$  represents the ideal  $DCG@p$ , computed from the correct ranking list. Here,  $r(i) = |\mathbf{y}_q \cap \mathbf{y}_i|$  indicates the similarity between the  $i$ -th item and the query.

#### 4.3.2 Jaccard-Similarity Based Metrics

Jaccard-based metrics assess semantic similarity between query and database images using the Jaccard similarity matrix, ranking results by label overlap. Following the multi-label retrieval protocol in [6], three measures are used: mean Average Precision ( $mAP$ ), normalized Discounted Cumulative Gain ( $nDCG$ ), and weighted Average Precision ( $wAP$ ). The  $mAP$  is computed under three thresholds (**Easy: 0.40, Medium: 0.60, Hard: 0.80**) to capture different levels of label overlap. The  $nDCG$  measures ranking quality using graded Jaccard relevance and is reported at  $k = 100$ . The



(a) DLRSD example 1

(b) DLRSD example 2

Figure 4: Examples of data augmentations applied to the DLRSD dataset.



(a) ML-AID example 1

(b) ML-AID example 2

Figure 5: Examples of data augmentations applied to the ML-AID dataset.



(a) WHDL D example 1

(b) WHDL D example 2

Figure 6: Examples of data augmentations applied to the WHDL D dataset.

wAP measures global precision weighted by the number of shared labels, without requiring a fixed relevance threshold, also at  $k = 100$ .

**Mean Average Precision (mAP)** Let  $Q$  be the number of queries. The mAP is given by:

$$\text{mAP} = \frac{1}{Q} \sum_q \text{AP}(q), \quad (13)$$

where AP the average precision for a query  $q$  is:

$$\text{AP}(q) = \frac{1}{N_{\phi(q)}@k} \sum_i^k \phi(q, i) \frac{N_{\phi(q)}@i}{i} \quad (14)$$

where  $\phi(q, i)$  is the indicator function for query  $q$  and the  $i$ -th image, and  $N_{\phi(q)}@k$  is the number of positive images in the top- $k$  ranks. Three settings for  $\phi$  have been used to assess image matching difficulty: *Easy*, *Medium*, and *Hard*, with Jaccard Index thresholds of 0.40, 0.60, and 0.80, respectively. These protocols evaluate performance under varying label counts, enable intuitive result interpretation, and emphasize label similarity in ML-RSIR and correct ranking (higher Jaccard Index ranked higher).

**Normalized Discounted Cumulative Gain (nDCG)** The nDCG is suitable for multilabel retrieval tasks, as it evaluates the relevance of the top-ranked results. It is defined at  $k$  as

$$\text{nDCG}@k = \frac{\text{DCG}@k}{\text{IDCG}@k} \quad (15)$$

where the DCG@ $k$  for a query  $q$  is

$$\text{DCG}@k = \sum_{i=1}^k \frac{2^{J(q,i)} - 1}{\log_2(i+1)} \quad (16)$$

with  $J(q, i)$  denoting the Jaccard Index between the query and the  $i$ -th ranked image. The ideal discounted cumulative gain (IDCG@ $k$ ) is computed as

$$\text{IDCG}@k = \sum_{i=1}^k \frac{2^{J(q,i)_r} - 1}{\log_2(i+1)} \quad (17)$$

where  $J(q, i)_r$  is the Jaccard Index between the query and the  $i$ -th ranked image, sorted in decreasing order of relevance  $r$ . The nDCG value ranges from zero to one, making results and comparisons more interpretable.

Table 4: Retrieval results for DLRSD where red and blue indicate the highest and second highest values respectively.

Method	Cosine Similarity-Based		Relevance-Based Jaccard Similarity				
	mAP(sim)@5000	nDCG(sim)@100	mAP Threshold			nDCG@100	wAP@100
			Easy@0.4	Medium@0.6	Hard@0.8		
SupCon ALL [14]	68.72	71.14	30.12	13.45	5.32	73.27	14.30
SupCon ANY [14]	68.43	69.85	30.13	13.55	5.49	72.42	13.76
LBase [38]	69.14	71.43	<b>30.36</b>	13.47	5.12	74.00	14.31
LProto [39]	70.03	73.14	30.25	13.71	5.43	74.47	15.34
LMsc [38]	69.09	71.54	30.14	13.41	5.27	74.15	14.82
OML [6]	73.27	76.08	29.28	13.13	5.07	71.58	<b>18.17</b>
MulSupCon [15]	69.71	72.51	29.70	13.27	5.01	74.43	14.67
Wg-MulSupCon [15]	70.32	73.50	<b>30.34</b>	13.69	5.47	<b>74.88</b>	15.17
Sim-Dis Loss [16]	67.74	70.01	30.12	13.55	5.31	72.67	13.37
LReg [17]	<b>75.23</b>	<b>77.60</b>	29.64	13.60	<b>5.96</b>	74.69	<b>15.57</b>
L-W/O-Reg [17]	70.88	73.68	30.25	<b>13.72</b>	5.58	74.72	15.27
<b>MACL (Ours)</b>	72.14	75.17	28.95	<b>14.28</b>	<b>6.85</b>	73.92	16.13
<b>Wg-MACL (Ours)</b>	<b>77.71</b>	<b>80.20</b>	29.26	13.19	5.31	<b>77.88</b>	<b>19.13</b>

**Weighted Average Precision (wAP)** The weighted Average Precision (wAP) metric is analogous to mAP, but incorporates the number of shared classes between the query and each retrieved image in its computation. This makes it applicable to ML-RSIR without requiring a predefined threshold for the indicator function. The wAP is therefore calculated as

$$\text{wAP} = \frac{1}{Q} \sum_q \frac{1}{N_\phi(q)@k} \sum_i^k \phi(q, i) \left( \frac{1}{i} \sum_j^i J(q, j) \right) \quad (18)$$

## 5 Results and Discussion

### 5.1 Quantitative Results

The quantitative evaluation is organised per dataset. Retrieval performance is reported using cosine similarity-based metrics and relevance-based Jaccard measures in order to capture both global embedding quality and threshold-dependent retrieval behaviour.

The retrieval results for the DLRSD, ML-AID, and WHDL D datasets are presented in Tables 4, 5, and 6, respectively. Through these evaluations, comparisons across different dataset scales, label diversity levels, and scene complexity are enabled. Multiple baseline and state-of-the-art retrieval methods were evaluated, and retrieval behaviour based on both cosine similarity and jaccard relevance was assessed. These variations across datasets facilitate a comprehensive assessment of retrieval robustness and generalisation.

Across all three datasets, the proposed MACL is consistently shown to outperform competing methods in the majority of evaluation metrics, demonstrating strong generalisation ability. The results further indicate that more discriminative and semantically consistent embeddings are learned by MACL. Improvements for rare categories may be attributed to the adaptive weighting and dynamic-temperature mechanisms, through which balanced retrieval performance is maintained across both frequent and infrequent land-cover classes.

#### 5.1.1 DLRSD Results

As shown in Table 4, both MACL and its weighted variant achieve strong and consistent performance across nearly all evaluation metrics. Weighted MACL attains clear gains in cosine similarity-based measures, while MACL performs best in relevance-based ranking, particularly at higher difficulty levels. The results indicate that the proposed approach maintains robust retrieval quality across varying similarity thresholds. Minor differences at the Easy and Medium levels suggest that MACL remains competitive even when other methods briefly outperform it, reflecting stable and balanced behavior across evaluation settings.

Table 5: Retrieval results for ML-AID where red and blue indicate the highest and second highest values respectively.

Method	Cosine Similarity-Based		Relevance-Based Jaccard Similarity				
	mAP(sim)@5000	nDCG(sim)@100	mAP Threshold			nDCG@100	wAP@100
			Easy@0.4	Medium@0.6	Hard@0.8		
SupCon ALL [14]	86.95	89.32	56.36	37.06	14.60	84.33	30.75
SupCon ANY [14]	87.20	86.31	56.95	37.75	<b>14.93</b>	82.22	26.90
LBase [38]	88.98	89.96	55.47	36.32	14.21	84.39	31.14
LProto [39]	88.41	89.64	56.18	36.94	14.73	83.98	30.28
LMsc [38]	89.10	89.77	56.33	36.96	14.51	83.83	29.71
OML [6]	93.13	93.52	57.90	<b>38.20</b>	<b>15.00</b>	67.61	36.78
MulSupCon [15]	89.62	90.09	55.56	36.63	14.46	84.61	30.84
Wg-MulSupCon [15]	90.11	90.21	56.24	36.81	14.44	84.43	30.60
Sim-Dis Loss [16]	88.36	89.04	56.91	37.37	14.76	58.04	29.45
LReg [17]	91.88	92.56	56.35	36.86	14.73	85.94	32.95
L-W/O-Reg [17]	91.81	92.76	56.24	36.56	14.15	<b>87.85</b>	36.98
<b>MACL (Ours)</b>	<b>95.77</b>	<b>95.90</b>	<b>59.89</b>	<b>38.86</b>	14.91	77.12	<b>43.84</b>
<b>Wg-MACL (Ours)</b>	<b>94.46</b>	<b>94.43</b>	<b>58.20</b>	37.94	14.54	<b>89.84</b>	<b>39.42</b>

Table 6: Retrieval results for WHDL D dataset. Red values indicate the highest performance among all methods, while blue values indicate the second highest.

Method	Cosine Similarity-Based		Relevance-Based Jaccard Similarity				
	mAP(sim)@5000	nDCG(sim)@100	mAP Threshold			nDCG@100	wAP@100
			Easy@0.4	Medium@0.6	Hard@0.8		
SupCon ALL [14]	90.87	92.77	82.86	66.66	42.26	78.06	61.54
SupCon ANY [14]	92.99	92.22	82.22	66.02	41.53	74.48	57.12
LBase [38]	93.23	92.46	82.81	<b>67.32</b>	<b>43.22</b>	76.59	59.78
LProto [39]	90.62	92.47	82.91	66.45	41.75	73.90	56.50
LMsc [38]	93.87	92.59	82.21	66.34	41.98	77.20	60.48
OML [6]	92.65	91.22	81.43	64.78	40.36	70.80	52.37
MulSupCon [15]	93.46	92.23	<b>83.15</b>	67.09	42.60	74.53	57.72
Wg-MulSupCon [15]	93.83	92.69	82.63	66.98	42.81	76.72	60.08
Sim-Dis Loss [16]	89.77	90.42	82.64	66.52	42.05	69.71	52.35
LReg [17]	90.71	89.68	82.10	65.88	41.49	65.94	47.50
L-W/O-Reg [17]	93.88	92.62	82.74	67.22	<b>43.26</b>	76.28	59.63
<b>MACL (Ours)</b>	<b>94.41</b>	<b>93.72</b>	82.54	66.22	42.31	<b>79.42</b>	<b>63.24</b>
<b>Wg-MACL (Ours)</b>	<b>94.14</b>	<b>93.55</b>	<b>83.23</b>	<b>67.45</b>	43.10	<b>78.20</b>	<b>61.90</b>

### 5.1.2 ML-AID Results

According to Table 5, MACL attains the most consistent overall performance on the ML-AID dataset, confirming its strong generalization on large-scale and diverse remote sensing data. It leads across most similarity- and relevance-based measures, showing effective feature learning and ranking precision. Although a few baselines achieve slightly higher values in isolated metrics, MACL maintains a more uniform advantage across thresholds, highlighting its ability to capture complex semantic relations within multi-label aerial imagery.

### 5.1.3 WHDL D Results

From Table 6, MACL and Weighted MACL obtain the highest or near-highest results across all evaluation criteria. Weighted MACL achieves stronger retrieval performance at lower similarity thresholds, while MACL yields superior ranking quality. This complementary trend suggests that the weighted variant enhances precision in easier retrieval conditions, whereas MACL offers more reliable ranking at challenging levels. Overall, both versions of MACL sustain leading performance across different retrieval perspectives and dataset conditions.

### 5.2 Qualitative Results

A qualitative comparison of retrieval performance on the DLRSD dataset is presented to complement the quantitative evaluation. For a fixed query image, the top-6 retrieved samples produced by each method are shown in Figure 7. Through this visualization, the effect of the loss function on the semantic relevance of the retrieved images can be observed. Methods that more effectively encode multi-label relationships tend to retrieve samples whose label sets closely correspond to those of the query image, whereas less effective methods often return visually similar yet semantically unrelated samples. These qualitative observations provide additional insight into the behaviour of the evaluated loss functions and help clarify performance differences that may not be fully captured by numerical metrics alone.

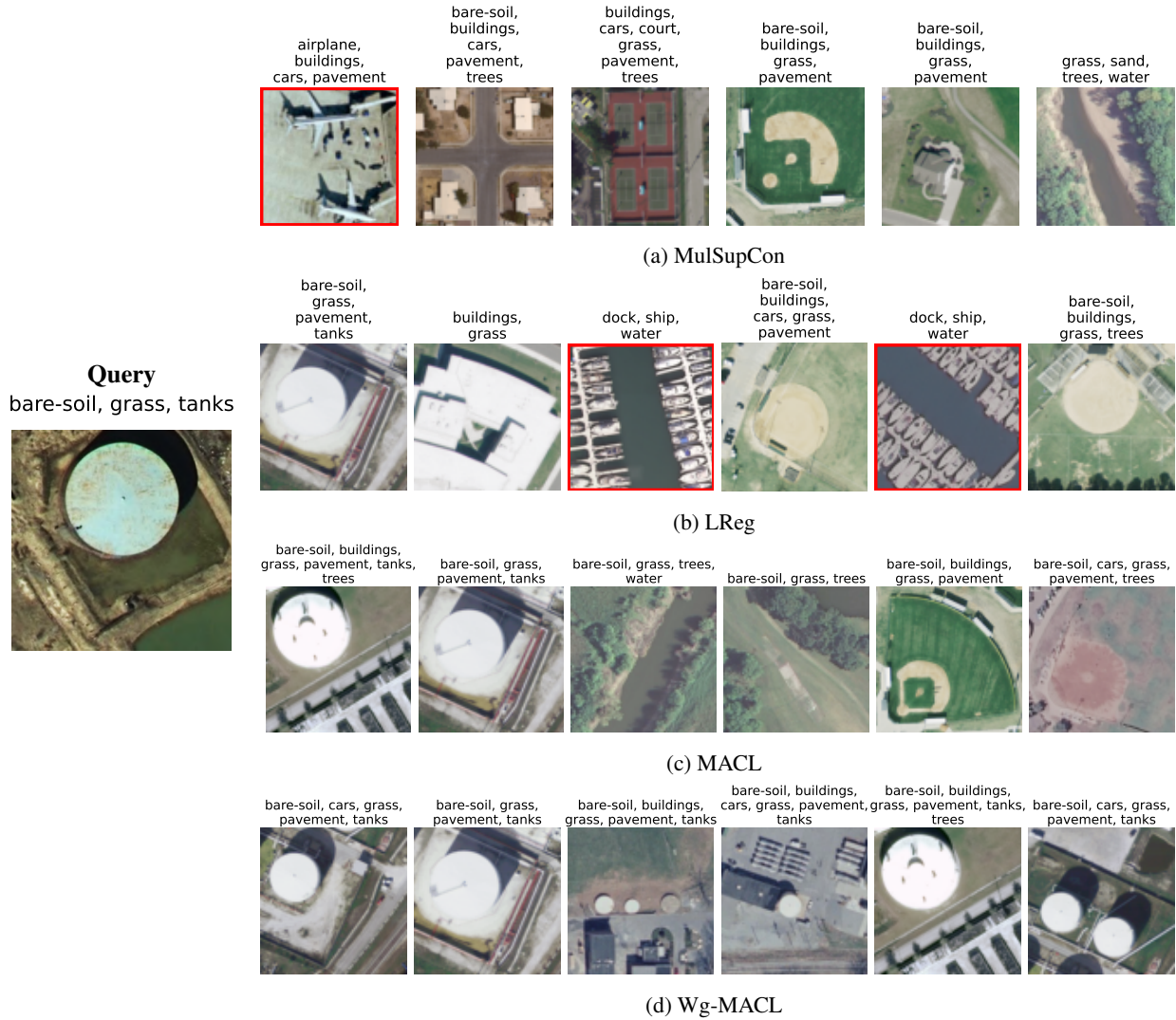


Figure 7: Top-6 retrieved images for the given query on the DLRSD dataset, comparing the best-performing methods (MulSupCon and LReg).

### 5.3 Discussion

The experimental results across all datasets demonstrate that MACL and its weighted variant consistently deliver improvements in multi-label remote sensing image retrieval. These gains are evident across cosine similarity-based metrics, relevance-based measures, and the qualitative retrieval examples. Several key observations can be drawn from these findings.

First, the consistent advantage of MACL across multiple evaluation metrics indicates that its adaptive mechanisms effectively address the limitations identified in the comparative study. In particular, the pairwise label reweighting component appears to mitigate the effects of class imbalance, enabling rare classes to exert greater influence during optimisation. This behaviour is reflected in the improved retrieval quality observed for infrequent land-cover categories, where baseline methods typically struggle.

Second, the dynamic temperature scaling mechanism is shown to improve the modelling of partial semantic similarity. By assigning temperature values based on label-overlap strength, the contrastive objective becomes more sensitive to nuanced relationships between samples. This results in embeddings that position semantically related images closer together while preventing visually similar but semantically unrelated samples from being mistakenly grouped. The observed improvements in nDCG and high-threshold mAP metrics particularly highlight the benefits of this adaptive formulation.

Third, the qualitative retrieval examples reinforce the quantitative trends by demonstrating clearer semantic alignment between query images and the top-ranked results produced by MACL-based models. These retrieved samples exhibit stronger agreement in label composition and scene characteristics compared to the outputs of competing loss functions. Such behaviour suggests that MACL produces a feature space that more faithfully represents the multi-label structure of remote sensing imagery.

Finally, the complementary behaviour observed between MACL and its weighted variant suggests that the proposed framework is flexible and can be tailored to different retrieval objectives. The weighted version performs especially well under lower similarity thresholds, whereas MACL itself yields superior ranking quality under stricter relevance conditions. This adaptability highlights the generalisability of the framework across diverse datasets and retrieval requirements.

Overall, the collective results confirm that MACL provides a robust and general-purpose solution for multi-label remote sensing image retrieval. The integration of frequency-aware weighting and adaptive temperature scaling leads to more discriminative, semantically coherent, and retrieval-effective feature representations compared to existing contrastive learning approaches.

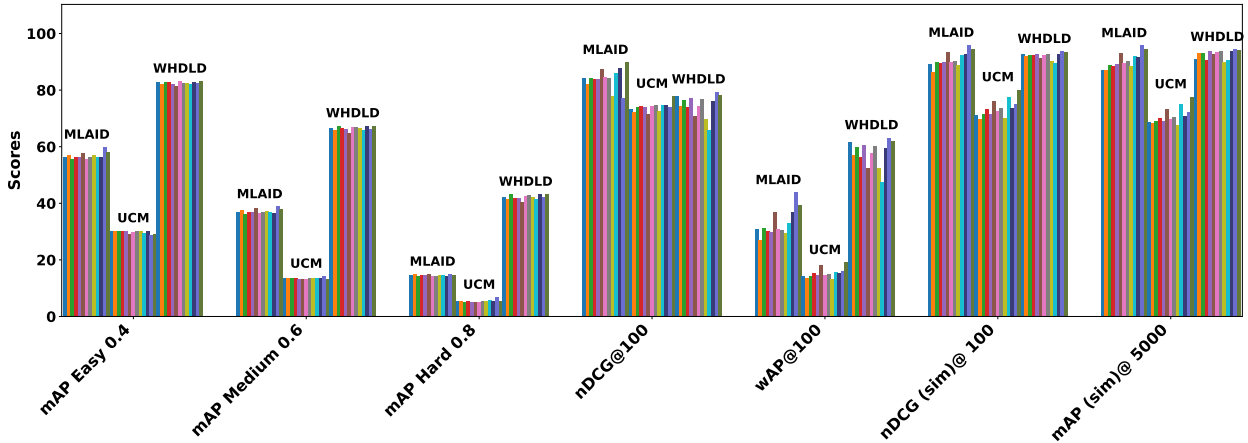


Figure 8: Loss Function Comparison Across Metrics (All Datasets). The evaluated loss functions are color-coded as follows: SupCon ALL (■), SupCon ANY (■), LBase (■), LProto (■), LMsc (■), OML (■), MulSupCon (■), Wg-MulSupCon (■), Sim-Dis Loss (■), LReg (■), L-W/O-Reg (■), MACL Loss (■), and Weighted MACL Loss (■).

## 5.4 Ablation Studies

To better understand the contribution of different design choices in the proposed framework, Ablation experiments were performed by varying the loss parameters, specifically the weighting term  $w_{ip}$  and the dynamic temperature  $T_{ip}$ , which is parameterized by the scaling factors  $\alpha$  and  $\beta$ . Different global temperature values and learning rate schedulers have also been tested.

For these studies, the analysis was restricted to the **DLRSD dataset**. This choice was guided by two factors. First, the ablation study required extensive parameter sweeps and repeated training runs, making it computationally impractical to conduct across all datasets. Second, DLRSD is one of the most widely used benchmarks in the ML-RSIR literature

and has been adopted in numerous prior studies. It therefore provides a representative and reliable basis for evaluating the design choices while keeping the experimental cost tractable.

The following subsections present detailed ablation results.

#### 5.4.1 Effect of $\alpha$ and $\beta$ in $w_{ip}$ and $T_{ip}$

To investigate the interaction between the weighting and temperature scaling mechanisms, an ablation analysis was conducted to examine the influence of the scaling factors  $\alpha$  and  $\beta$  on the retrieval performance.

Four configurations were considered: (i)  $\alpha$ - $\beta$  in  $T_{ip}$  without  $w_{ip}$ , (ii) the combined  $w_{ip} + T_{ip}$  case, (iii)  $w_{ip}$  with  $\alpha$ , and (iv)  $w_{ip}$  with  $\beta$ . The results are summarized in Fig. 9.

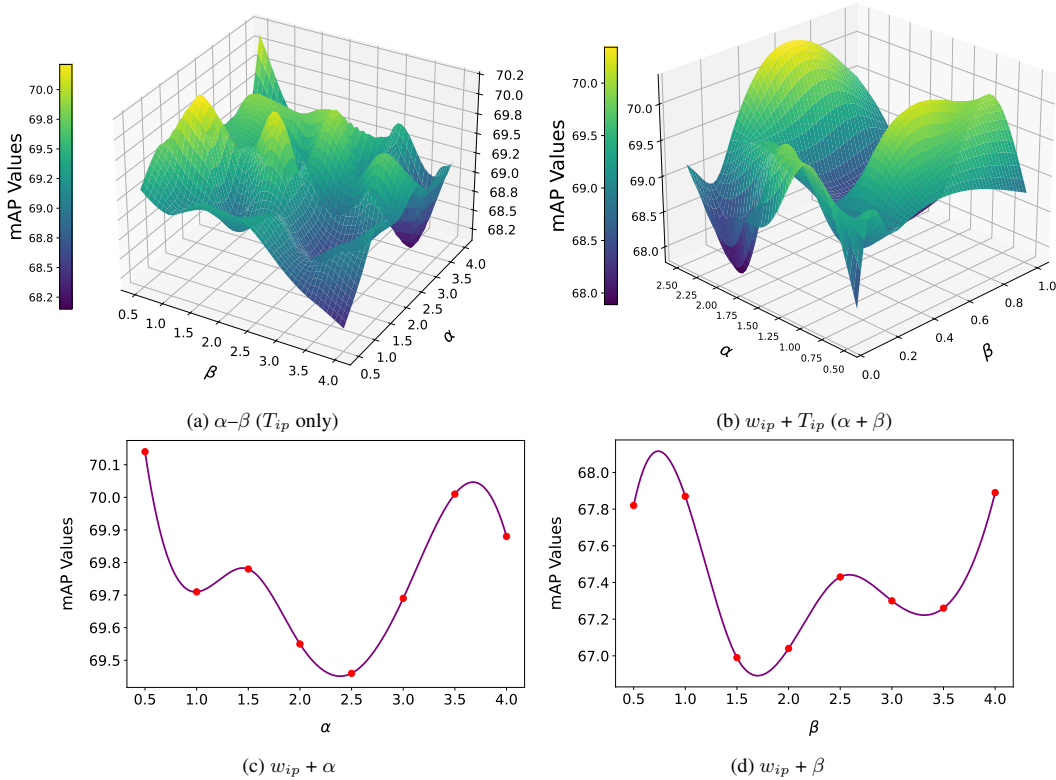


Figure 9: Ablation study on the role of  $T_{ip}$  (parameterized by  $\alpha$  and  $\beta$ ) and  $w_{ip}$  in the proposed MACL loss. Subfigures (a) and (b) show mAP performance as 3D surfaces (with colorbars indicating mAP in %), while (c) and (d) show 2D mAP curves for varying  $\alpha$  and  $\beta$ , respectively: (a) mAP Performance vs  $\alpha$  and  $\beta$  ( $T_{ip}$  only), (b) mAP Performance vs  $w_{ip}$  and  $T_{ip}$  ( $\alpha + \beta$ ), (c) mAP vs  $w_{ip}$  and  $\alpha$ , and (d) mAP vs  $w_{ip}$  and  $\beta$ .

When either the weighting or temperature modules are removed, a noticeable reduction in retrieval performance is observed, confirming that semantic consistency and category balance are enhanced through these mechanisms. The design rationale of MACL is validated by these findings, and its ability to produce well-balanced representations is supported by the observed results.

#### Effect of $T_{ip}$ Only ( $\alpha + \beta$ )

As shown in Fig. 9(a), the variation of  $\alpha$  and  $\beta$  under the  $T_{ip}$  only condition resulted in mAP values ranging from 68.1% to 70.2%, with the highest value observed at ( $\alpha=1.5, \beta=1.0$ ). Moderate scaling was found to enhance representation learning, whereas extreme values reduced accuracy due to excessive temperature adjustment. These findings indicate that  $T_{ip}$  provides a positive contribution when appropriately balanced.

### Effect of $w_{ip}$ and $T_{ip}$

In Fig. 9(b), the combination of  $w_{ip}$  and  $T_{ip}$  is shown to produce smoother and higher performance, with the maximum mAP recorded near 69.9%. The complementarity of the two modules is demonstrated, as  $w_{ip}$  improves sample weighting and  $T_{ip}$  adaptively regulates contrast strength, resulting in enhanced stability and retrieval accuracy.

### Effect of $w_{ip}$ with $\alpha$

From Fig. 9(c), the mAP reached its highest value of 70.1% when  $\alpha$  was approximately 0.5, after which a gradual decline was observed. Moderate values of  $\alpha$  were found to provide the best balance between informative and redundant pairs, while larger  $\alpha$  values placed excessive emphasis on strong pair relations, thereby reducing generalization.

### Effect of $w_{ip}$ with $\beta$

As shown in Fig. 9(d),  $\beta$  exhibited a sharper sensitivity, with an optimal mAP of 67.9% observed near  $\beta \approx 1.0$ . Larger  $\beta$  values were found to destabilize weighting, confirming that moderate scaling results in more consistent representations within the MACL framework.

## 5.4.2 Effect of Temperature Parameter

The temperature parameter  $\tau$  is a critical factor in supervised contrastive learning, as it regulates the sharpness of similarity distributions. To evaluate its impact, an ablation study has been conducted with  $\tau \in \{0.1, 0.2, 0.3\}$  across three benchmark datasets: DLRSD, ML-AID, and WHDL. Very low values (e.g.,  $\tau < 0.09$ ) led to embedding collapse, where learned representations became indistinguishable, and were therefore omitted from the analysis.

As shown in Fig. 10, the mAP performance consistently improves as  $\tau$  increases from 0.1 to 0.3.

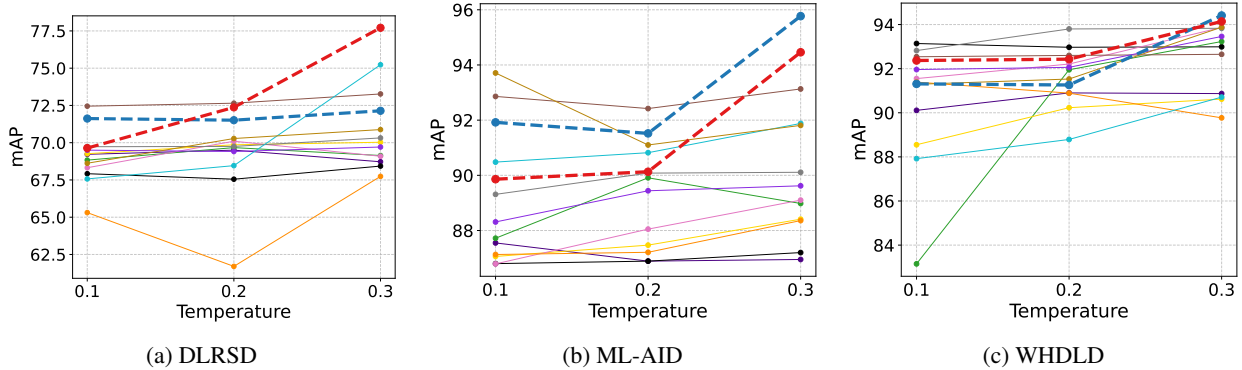


Figure 10: Ablation study of the temperature parameter  $\tau \in \{0.1, 0.2, 0.3\}$  vs. mAP across three datasets (DLRSD, ML-AID, and WHDL). The evaluated loss functions are color-coded as follows: SupCon ALL (■), SupCon ANY (■), LBase (■), LProto (■), LMsc (■), OML (■), MulSupCon (■), Wg-MulSupCon (■), Sim-Dis Loss (■), LReg (■), L-W/O-Reg (■), MACL Loss (■), and Weighted MACL Loss (■).

This trend highlights the stabilizing effect of higher temperature on contrastive optimization, reducing over-clustering of positive pairs and enhancing retrieval quality. The highest performance across all datasets is achieved at  $\tau = 0.3$ , which was consequently selected as the default for all subsequent experiments.

This observation aligns with prior work in remote sensing contrastive learning, where  $\tau = 0.3$  was identified as a robust and stable benchmark that balances optimization dynamics and generalization performance[12, 43].

## 5.4.3 Effect of Pretrained Weights on ResNet-18 Backbone

To analyze the role of pretrained weights, the proposed MACL and Weighted MACL losses were evaluated on ResNet-18 backbones with and without ImageNet initialization. Table(7) summarizes the results across the DLRSD, ML-AID, and WHDL datasets.

Several patterns can be observed. First, pretrained weights consistently improve retrieval performance across all datasets and loss variants. For example, on ML-AID, MACL with weights achieves an mAP(sim)@5000 of 95.77% compared

Table 7: Effect of pretrained ResNet-18 weights across three datasets for MACL and Weighted MACL. Results are reported with and without ImageNet weights.

Method	Loss	Pretrained	Cosine Similarity-Based		Relevance-Based Jaccard Similarity			nDCG@100	wAP@100
			mAP(sim)@5000	nDCG(sim)@100	mAP Threshold				
					Easy@0.4	Medium@0.6	Hard@0.8		
DLRSD	MACL Loss	Yes	72.14	75.17	28.95	<b>14.28</b>	<b>6.85</b>	73.92	16.13
		No	70.18	72.02	<b>29.89</b>	13.44	5.33	73.48	14.59
	Wg-MACL	Yes	<b>77.71</b>	<b>80.20</b>	29.26	13.19	5.31	<b>77.88</b>	<b>19.13</b>
		No	71.43	74.85	28.24	12.95	5.03	73.89	16.12
ML-AID	MACL Loss	Yes	<b>95.77</b>	<b>95.90</b>	<b>59.89</b>	<b>38.86</b>	<b>14.91</b>	77.12	<b>43.84</b>
		No	91.84	91.55	57.69	37.75	14.58	87.63	37.85
	Wg-MACL	Yes	94.46	94.43	58.20	37.94	14.54	<b>89.84</b>	39.42
		No	89.26	89.83	54.85	35.86	14.25	83.87	31.09
WHDL D	MACL Loss	Yes	94.41	93.72	82.54	66.22	42.31	<b>79.42</b>	<b>63.24</b>
		No	<b>94.50</b>	<b>93.89</b>	82.19	65.96	41.85	78.82	62.63
	Wg-MACL	Yes	94.14	93.55	<b>83.23</b>	<b>67.45</b>	<b>43.10</b>	78.20	61.90
		No	92.69	92.48	83.22	67.02	42.58	75.76	58.85

to 91.84% without weights. Second, the performance gap is more pronounced for Weighted MACL, indicating that pretrained initialization stabilizes the interaction between the loss components. Finally, although ResNet-18 is shallower than ResNet-50 or ResNet-101, the consistent improvements from pretrained initialization highlight its importance, particularly in remote sensing retrieval tasks where labeled training data is limited.

#### 5.4.4 Effect of Learning Rate

Learning rate plays a crucial role in determining convergence stability and final retrieval performance. Experiments were conducted with three values ( $LR \in \{0.1, 0.01, 0.001\}$ ) across the DLRSD, ML-AID, and WHDL D datasets, considering both MACL and Weighted MACL losses. The results are shown in Fig. 11.

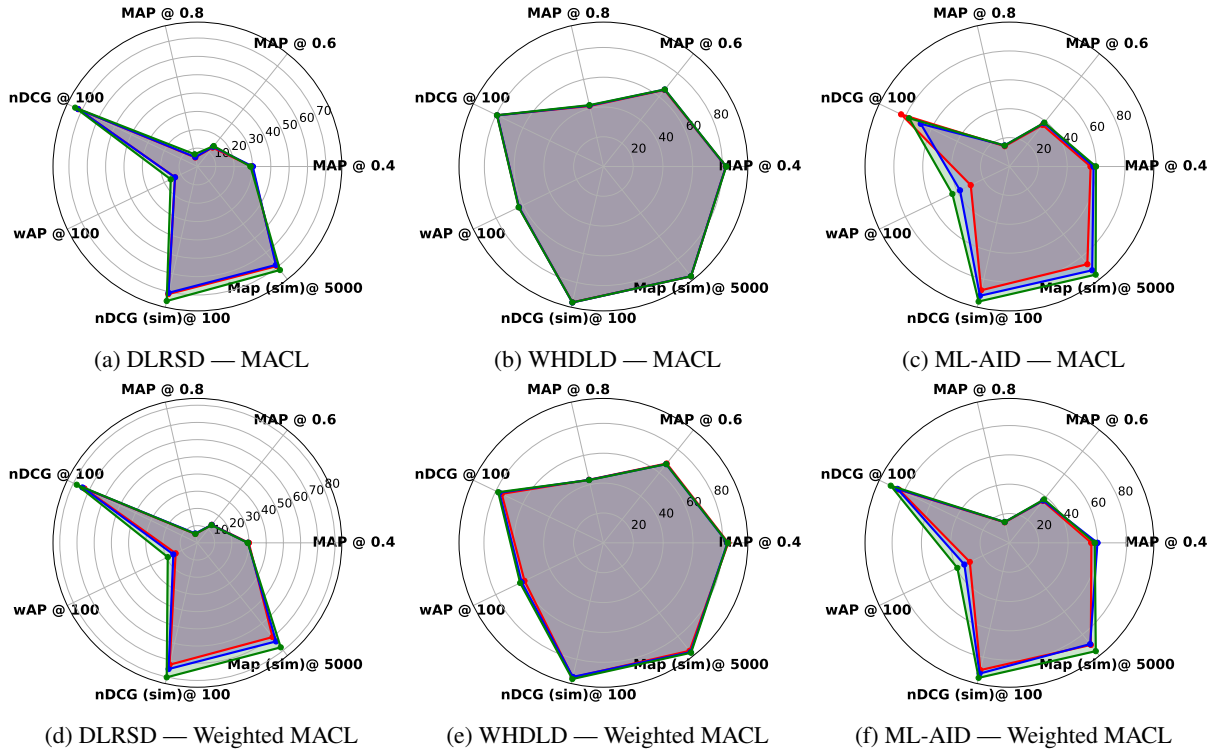


Figure 11: Effect of learning rate on MACL and Weighted MACL across datasets. Smaller learning rates generally achieve the best retrieval accuracy. Results are shown for LR = 0.1 (■), LR = 0.01 (■), LR = 0.001 (■).

Smaller learning rates ( $LR = 0.001$ ) consistently yield the strongest retrieval results. For example, on ML-AID with MACL,  $mAP(sim)@5000$  improves from 89.26% at  $LR = 0.1$  to 95.77% at  $LR = 0.001$ . Similarly, Weighted MACL on DLRSD increases from 70.08% at  $LR = 0.1$  to 77.71% at  $LR = 0.001$ .

Intermediate learning rates ( $LR = 0.01$ ) often provide stable but slightly lower scores than  $LR = 0.001$ . High learning rates ( $LR = 0.1$ ) generally degrade performance, particularly for Weighted MACL, as overly aggressive updates destabilize the balance between  $w_{ip}$  and  $T_{ip}$ .

The WHDL D dataset shows relative robustness, with all three learning rates achieving similar retrieval accuracy ( $mAP(sim)@5000 \approx 94\%$ ). This suggests that dataset scale and diversity mitigate sensitivity to the learning rate.

Overall, the ablation confirms that  $LR = 0.001$  provides the most effective trade-off between convergence and retrieval accuracy, and this value is adopted in all subsequent experiments.

## 6 Conclusion

This study introduced MACL loss, a loss tailored for multi-label CBIR in remote sensing. By integrating label-aware sampling, frequency-sensitive weighting, and dynamic temperature scaling, MACL effectively mitigates the challenges of imbalanced label distributions, semantic overlaps, and pairwise co-occurrence effects. Comprehensive experiments on the DLRSD, ML-AID, and WHDL D datasets show that MACL consistently surpasses existing supervised contrastive variants across multiple metrics, producing discriminative, balanced, and semantically coherent embeddings. The ablation analyses further confirm the role of each component, indicating that both the weighting and temperature mechanisms are essential for stable and high-quality retrieval performance and that MACL effectively achieves its design objectives.

Although MACL achieves strong performance, challenges remain in distinguishing visually similar classes (e.g., river vs. runway). Future work will focus on modeling higher-order label correlations, exploring multi-modal extensions, and adapting MACL for semi-supervised or weakly labeled settings.

## References

- [1] Liping Di and E. Yu. Big data analytics for remote sensing: Concepts and standards. In *Remote Sensing Big Data*, Springer Remote Sensing/Photogrammetry. Springer, Cham, 2023.
- [2] Ritendra Datta, Dhiraj Joshi, Jia Li, and James Z. Wang. Image retrieval: Ideas, influences, and trends of the new age. *ACM Computing Surveys (CSUR)*, 40(2):1–60, 2008.
- [3] Weixun Zhou, Haiyan Guan, Ziyu Li, Zhenfeng Shao, and Mahmoud R. Delavar. Remote sensing image retrieval in the past decade: Achievements, challenges, and future directions. *IEEE JSTARS*, 16(1), 2023.
- [4] G. Sumbul, M. Ravanbakhsh, and B. Demir. A relevant, hard and diverse triplet sampling method for multi-label remote sensing image retrieval. In *Proceedings of the IEEE Mediterranean and Middle-East Geoscience and Remote Sensing Symposium (M2GARSS)*, pages 1–5, 2022.
- [5] G. Sumbul, M. Ravanbakhsh, and B. Demir. Informative and representative triplet selection for multilabel remote sensing image retrieval. *IEEE TGRS*, 60:1–11, 2022.
- [6] R. Imbriaco, C. Sebastian, E. Bondarev, and P. H. N. de With. Toward multilabel image retrieval for remote sensing. *IEEE TGRS*, 60, July 2022.
- [7] Z. Shao, W. Zhou, X. Deng, M. Zhang, and Q. Cheng. Multilabel remote sensing image retrieval based on fully convolutional network. *IEEE JSTARS*, 13:318–328, 2020.
- [8] L. Han et al. Hash-based remote sensing image retrieval. *IEEE TGRS*, 62:1–23, 2024.
- [9] Peng Li, Lirong Han, Xuanwen Tao, Xiaoyu Zhang, Christos Grecos, Antonio Plaza, and Peng Ren. Hashing nets for hashing: A quantized deep learning to hash framework for remote sensing image retrieval. *IEEE Transactions on Geoscience and Remote Sensing*, 58(10):7331–7345, October 2020.
- [10] J. Kang, R. Fernandez-Beltran, D. Hong, J. Chanussot, and A. Plaza. Graph relation network: Modeling relations between scenes for multilabel remote-sensing image classification and retrieval. *IEEE TGRS*, 59(5):4355–4369, May 2021.
- [11] Ting Chen, Simon Kornblith, Mohammad Norouzi, and Geoffrey Hinton. A simple framework for contrastive learning of visual representations. In *Proceedings of the 37th International Conference on Machine Learning*. PMLR, 2020.

- [12] Qiyang Liu, Yun Ge, Sijia Wang, Ting Wang, and Jinlong Xu. Dynamic-manifold-based sample selection in contrastive learning for remote sensing image retrieval. *The Visual Computer*, 41:4111–4127, 2025.
- [13] Mengluan Huang, Le Dong, Weisheng Dong, and Guangming Shi. Supervised contrastive learning based on fusion of global and local features for remote sensing image retrieval. *IEEE TGRS*, 61:1–15, 2023.
- [14] P. Khosla, P. Teterwak, C. Wang, A. Sarna, Y. Tian, P. Isola, A. Maschinot, C. Liu, and D. Krishnan. Supervised contrastive learning. *Advances in Neural Information Processing Systems (NeurIPS)*, 2021.
- [15] P. Zhang and M. Wu. Multi-label supervised contrastive learning. In *Proceedings of the AAAI Conference on Artificial Intelligence*, volume 38, pages 16786–16793, Vancouver, Canada, 2024.
- [16] Guangming Huang, Yunfei Long, Cunjin Luo, and Sheng Liu. Similarity-dissimilarity loss for multi-label supervised contrastive learning. *arXiv preprint arXiv:2410.13439*, 2024.
- [17] Alexandre Audibert, Aurélien Gauffre, and Massih-Reza Amini. Multi-label contrastive learning: A comprehensive study. In *Proceedings of the European Conference on Machine Learning and Principles and Practice of Knowledge Discovery in Databases (ECML PKDD)*, Ghent, Belgium, 2024. Springer.
- [18] M. Zhang, Q. Cheng, F. Luo, and L. Ye. A triplet nonlocal neural network with dual anchor triplet loss for high resolution remote sensing image retrieval. *IEEE JSTARS*, 14:2711–2723, 2021.
- [19] Rui Cao, Qian Zhang, Jiasong Zhu, Qing Li, Qingquan Li, Bozhi Liu, and Guoping Qiu. Enhancing remote sensing image retrieval using a triplet deep metric learning network. *International Journal of Remote Sensing*, 41(2):740–751, 2019.
- [20] H. Zhao, L. Yuan, H. Zhao, and Z. Wang. Global aware ranking deep metric learning for remote sensing image retrieval. *IEEE GRSL*, 19:8008505, 2022.
- [21] L. Fan, H. Zhao, and H. Zhao. Global optimization: Combining local loss with result ranking loss in remote sensing image retrieval. *IEEE TGRS*, 59(8):7011–7026, 2021.
- [22] Y. Wang, S. Ji, and Y. Zhang. A learnable joint spatial and spectral transformation for high resolution remote sensing image retrieval. *IEEE JSTARS*, 14:8100–8112, 2021.
- [23] S. Wang, D. Hou, and H. Xing. A novel multi attention fusion network with dilated convolution and label smoothing for remote sensing image retrieval. *International Journal of Remote Sensing*, 43(4):1306–1322, 2022.
- [24] U. Chaudhuri, B. Banerjee, A. Bhattacharya, and M. Datcu. Attention driven graph convolution network for remote sensing image retrieval. *IEEE GRSL*, 19:8019705, 2022.
- [25] Jiahui Wu, Zhuowei Wang, Genping Zhao, and Shuo Qu. A self-attention feature metric learning method for remote sensing image retrieval. In *Proceedings of the 2023 15th International Conference on Machine Learning and Computing (ICMLC '23)*, pages 399–405, 2023.
- [26] W. Song, Z. Gao, R. Dian, P. Ghamisi, Y. Zhang, and J. A. Benediktsson. Asymmetric hash code learning for remote sensing image retrieval. *IEEE TGRS*, 60:5617514, 2022.
- [27] X. Tang et al. Meta hashing for remote sensing image retrieval. *IEEE TGRS*, 60:5615419, 2022.
- [28] Rui Wang, Jian Zheng, Wei Zhou, Qi Wang, Yan Lu, and Yujian Tao. Adaptive hash code balancing for remote sensing image retrieval. *International Journal of Remote Sensing*, 44(2):690–712, 2023.
- [29] G. Sumbul and B. Demir. Plasticity stability preserving multi task learning for remote sensing image retrieval. *IEEE TGRS*, 60:5620116, 2022.
- [30] Z. Li, M. Chen, and K. Huang. Centripetal intensive deep hashing for remote sensing image retrieval. *IEEE JSTARS*, 18:12439–12450, 2025.
- [31] Yichao Zhang, Xiangtao Zheng, and Xiaoqiang Lu. Remote sensing image retrieval by deep attention hashing with distance-adaptive ranking. *IEEE JSTARS*, 16:4301–4314, 2023.
- [32] W. Zhou, X. Deng, and Z. Shao. Region convolutional features for multi-label remote sensing image retrieval. *arXiv preprint arXiv:1807.08634*, 2020.
- [33] ShengWu Fu, ZhengShen Gu, Dong Wang, and Songhua Xu. Generative contrastive learning for multi-label image classification. In *Proceedings of the 2024 International Symposium on Digital Home (ISDH)*, pages 1–6. IEEE, 2024.
- [34] B. Chaudhuri, B. Demir, S. Chaudhuri, and L. Bruzzone. Multilabel remote sensing image retrieval using a semisupervised graph-theoretic method. *IEEE TGRS*, 56(2):1144–1158, 2018.
- [35] G. Sumbul and B. Demir. A novel graph-theoretic deep representation learning method for multi-label remote sensing image retrieval. In *Proceedings of the IEEE IGARSS*, pages 266–269, 2021.

- [36] O. E. Dai, B. Demir, B. Sankur, and L. Bruzzone. A novel system for content based retrieval of multi-label remote sensing images. In *Proc. IEEE IGARSS*, pages 1744–1747, 2017.
- [37] Y. Hua, X. X. Zhu, and L. Mou. A pairwise label inference network for multi-label aerial image analysis. *IEEE TGRS*, 2021.
- [38] Alexandre Audibert, Aurélien Gauffre, and Massih-Reza Amini. Exploring contrastive learning for long-tailed multi-label text classification. In *European Conference on Machine Learning and Principles and Practice of Knowledge Discovery in Databases (ECML PKDD)*, pages 245–261, 2024.
- [39] Rohit Gupta, Anirban Roy, Claire Christensen, Sujeong Kim, Sarah Gerard, Madeline Cincebeaux, Ajay Divakaran, Todd Grindal, and Mubarak Shah. Class prototypes based contrastive learning for classifying multi-label and fine-grained educational videos. In *Proceedings of the IEEE/CVF Conference on Computer Vision and Pattern Recognition*, pages 19923–19933, 2023.
- [40] B. Chaudhuri, B. Demir, S. Chaudhuri, and L. Bruzzone. Multilabel remote sensing image retrieval using a semi supervised graph-theoretic model. *IEEE TGRS*, 56(2):1144–1158, 2018.
- [41] Y. Hua, L. Mou, and X. X. Zhu. Relation network for multilabel aerial image classification. *IEEE TGRS*, 58(7):4554–4570, 2020.
- [42] Yuan Cao, Xiangru Chen, Zifan Liu, Wenzhe Jia, Fanlei Meng, and Jie Gui. Deep continual hashing for real-world multi-label image retrieval. *Expert Systems with Applications*, 2023.
- [43] A. Amir and E. Aptoula. A comparative study of multi-label supervised contrastive losses for the content-based image retrieval of remote sensing images. In *Proceedings of the 2025 33rd Signal Processing and Communications Applications Conference (SIU)*, pages 1–4. IEEE, 2025.